A theoretical study for nanoparticle partitioning in the lamellae of diblock copolymers

Jiezhu Jin and Jianzhong Wu[a)]
Department of Chemical and Environmental Engineering, University of California, Riverside, California 92521, USA

(Received 5 September 2007; accepted 29 November 2007; published online 19 February 2008)

Morphology control is important for practical applications of composite materials that consist of functional polymers and nanoparticles. Toward that end, block copolymers provide useful templates to arrange nanoparticles in the scaffold of self-organized polymer microdomains. This paper reports theoretical predictions for the distribution of nanoparticles in the lamellar structures of symmetric diblock copolymers on the basis of a polymer density functional theory (DFT) and the potential distribution theorem (PDT). The DFT predicts periodic spacing of lamellar structures in good agreement with molecular dynamics simulations. With the polymer structure from DFT as the input, the PDT is used to examine the effects of particle size, surface energy, polymer chain length, and compressibility on the distribution of nanoparticles in the limit of low particle density. It is found that the nanoparticle distribution depends not only on the particle size and surface energy but also on the local structure of the microdomain interface, polymer chain length, and compressibility. The theoretical predictions are compared well with experiments and simulations. © *2008 American Institute of Physics*. [DOI: 10.1063/1.2827470]

I. INTRODUCTION

Many studies have been reported on the self-assembly of block copolymers with ordered microstructure on the length scale varying from a few nanometers to hundreds of nanometers. However, it remains primitive on the application of the ordered block-copolymer structures as templates for the organization of nanostructured materials such as those used in organic solar cells that require a precise control of the spatial distributions of organic and inorganic constituents from a molecular perspective. For block copolymer and nanoparticle mixtures, on the one hand, microphase separation of block copolymer promotes self-assembly of nanoparticles to produce highly ordered and thermodynamically stable hybrid materials. On the other hand, at a finite particle concentration, the nanoparticles modify the characteristic dimensions or the morphology of the ordered block-copolymer structures.[1,2] Synergistic interactions between nanoparticles and block-copolymer matrix lead to hierarchically structured composites that offer benefits such as enhanced electrical conductivity, improved heat resistance, and controllable gas permeability.[1–4]

Design and fabrication of particle-copolymer nanocomposites require a fundamental understanding of particle organization in the block-copolymer matrices. Toward that end, a number of theoretical and simulation studies have been reported.[3,5–8,13,14] For example, Wang *et al.* used lattice Monte Carlo simulations to examine the location of a singe nanoparticle in the lamellae of symmetric diblock copolymers.[3] They found that nanoparticles are favorably localized at the microdomain interface if there is no energetic preference, but are engulfed in an energetically preferential microdomain otherwise. More systematic investigations have been reported by Balazs and co-workers by using a theoretical method that combines the self-consistent-field theory (SCFT) for block copolymers and a density functional theory (DFT) for nanoparticles.[5–8] These researchers examined in detail how the properties of the polymers and particles influence the morphology of polymer nanocomposite systems in the bulk and under confinement.[5–8] Qualitatively, the theoretical predictions have been confirmed by a number of experimental studies on the entropically or enthalpically driven segregations of particles within the block-copolymer matrices.[1,9–12] More recently, similar predictions were reported on the basis of analytical theories for various simplified coarse-grained polymer models.[13] To conciliate the incompressible model for polymers and the local packing effect of nanoparticles, Sides *et al.* combined the SCFT for polymers with Brownian dynamics (BD) simulation for particles.[14] They found that the SCFT/BD simulation predicts morphology in good agreement with experiments for the distribution of polystyrene (PS)-functionalized gold nanoparticles in a PS-poly(2-vinylpyridine) (PS-P2VP) diblock-copolymer melt.

In this work, we investigate the capacity of symmetric diblock copolymers for organization of nanoparticles in the limit of low particle concentration. The purpose is twofold. First, we intend to examine the numerical performance of a polymer DFT for predicting the microstructures of particle-block copolymer mixtures. We compare the theoretical predictions with the simulation data in the literature, with those from SCFT for the lamellar structures of block-copolymer melts, and with recent experiments on the distribution of nanoparticles in polymer structure. Second, we aim to establish a particle-based theoretical framework for predicting the

[a)]Electronic mail: jwu@engr.ucr.edu.

organization of nanoparticles at low concentration within the lamellae of block copolymers. Departing from earlier theoretical studies, we consider intermolecular interactions between polymer segments and nanoparticles explicitly. As in molecular simulations, our model accounts for polymers and particles within a single molecular framework. The particle-based polymer model allows us to describe all important factors affecting the nanoparticle distribution in a self-consistent manner.

The remainder of this article is organized as follows. After a brief introduction of the theoretical model, we test the numerical performance of the DFT by comparison with that of the SCFT and with "exact" results from molecular dynamics simulations. By using the potential distribution theorem (PDT), we investigate the partitioning of nanoparticles in the lamellar structures in terms of a range of molecular and thermodynamic parameters including the particle size and surface energy as well as the chain length, polymer packing density, and microdomain heterogeneity. Comparisons are also made with pertinent experimental/simulation results and with previous SCFT predictions.

II. MOLECULAR MODEL AND THEORETICAL BACKGROUND

Following a previous simulation work,[15] we consider binary mixtures of symmetric diblock copolymers and nanoparticles where the particles are represented by structureless spheres and the diblock copolymers are tangentially connected sphere chains. Each polymer chain consists of two types of segments, designated as "A" and "B," with the same size (or diameter σ_s) but different interaction energies. The average packing fraction of the polymer ($\eta=\pi\rho_{\text{av}}\sigma_s^3/6$, ρ_{av} is average polymer density) is larger than 0.3, close to that in a typical polymer melt. We use relatively short chains ($N=10,20$ segments per chain) for direct comparison with the simulation results but much longer chains ($N=100$ and 200) for investigating the distribution of nanoparticles.

The pair potential between copolymer segments and nanoparticles is described by a square-well model,

$$\varphi_{ij}(r)=\begin{cases}\infty, & r<\sigma_{ij}\\ -\varepsilon_{ij}, & \sigma_{ij}\leqslant r\leqslant\gamma\sigma_{ij}\\ 0, & r>\gamma\sigma_{ij},\end{cases} \tag{1}$$

where subscripts i and j denote a polymer segment or a nanoparticle, ε_{ij} represents the strength of the pair interaction energy, $\sigma_{ij}=(\sigma_i+\sigma_j)/2$ is the cross diameter, and γ specifies the range of attraction (or repulsion). As in the simulations,[15] we use $\gamma=2$ throughout this work.

In contrast to an early work that combines a lattice-based model for polymers and a continuous model for particles,[5–8] we treat the particle and polymer segments within the same molecular framework. Specifically, we consider the excluded-volume interactions between polymer segments of the same type (i.e., $\varepsilon_{\text{AA}}=\varepsilon_{\text{BB}}=0$) but impose a "square-shoulder" repulsion between different polymers $\varepsilon_{\text{AB}}<0$ to facilitate the microphase segregation. In addition to the excluded-volume effect, the interaction between a particle and polymer segments can be either repulsive or attractive.

In a previous work, we have developed a DFT applicable to particle-diblock copolymer mixtures.[16] Briefly, the Helmholtz energy functional includes an expression for the ideal chains that preserve the molecular topology and an excess arising from nonbonded intra- and intermolecular interactions. The excess part of the Helmholtz energy functional includes three contributions, accounting for the excluded-volume effects, correlations due to the chain connectivity, and short-range attraction/repulsion,[17]

$$\beta F_{\text{ex}}[\{\rho_j(\mathbf{r})\}]=\int d\mathbf{r}\{\phi^{hs}[n_\alpha(\mathbf{r})]+\phi^{\text{chain}}[n_\alpha(\mathbf{r})]\}+\beta F_{\text{ex}}^{\text{sw}}[\{\rho_j(\mathbf{r})\}], \tag{2}$$

where $\beta=1/k_BT$ with k_B being the Boltzmann constant and T the temperature; ϕ^{hs} and ϕ^{chain} are the Helmholtz energy densities due to the excluded-volume effects and the intrachain correlations, respectively; and $F_{\text{ex}}^{\text{sw}}$ is the Helmholtz energy due to the square-well interactions beyond the hard-sphere collision. The appendix gives expressions for the individual terms on the right side of Eq. (2). We refer to our previous publications for details.[18–21]

While the DFT is applicable to polymer-particle mixtures of arbitrary morphology, this work concerns only the distribution of nanoparticles within the lamellar structures of symmetric block copolymers. For simplicity, we consider the low concentration limit of nanoparticles such that their influence on the polymer structure is negligible. In that case, the density profiles of the diblock-copolymer segments are identical to those in the neat copolymer lamellae, which can be solved from the Euler-Lagrange equations,[17]

$$\rho_A(z)=\exp(\beta\mu_M)\sum_{i=A}G_L^i(z)\exp[-\beta\lambda_i(z)]G_R^i(z), \tag{3}$$

$$\rho_B(z)=\exp(\beta\mu_M)\sum_{i=B}G_L^i(z)\exp[-\beta\lambda_i(z)]G_R^i(z). \tag{4}$$

In Eqs. (3) and (4), z represents the direction perpendicular to the lamellae, μ_M stands for the polymer chemical potential, and $G_L^i(z)$ and $G_R^i(z)$ are, respectively, the left and right recurrence functions,

$$G_L^i(z)=\frac{1}{2\sigma_s}\int_{z-\sigma_s}^{z+\sigma_s}\exp[-\beta\lambda_{i-1}(z)]G_L^{i-1}(z)dz, \tag{5}$$

$$G_R^i(z)=\frac{1}{2\sigma_s}\int_{z-\sigma_s}^{z+\sigma_s}\exp[-\beta\lambda_{i+1}(z)]G_R^{i+1}(z)dz, \tag{6}$$

with the initial values $G_L^1(z)=1$ and $G_R^M(z)=1$. The self-consistent fields $\lambda_i(z)$ are related to the excess Helmholtz energy functional F_{ex} by

$$\lambda_A(z)=\frac{\delta F_{\text{ex}}}{\delta\rho_A(z)}, \tag{7}$$

$$\lambda_B(z)=\frac{\delta F_{\text{ex}}}{\delta\rho_B(z)}. \tag{8}$$

Given an average polymer density, Eqs. (3)–(8) are solved with the periodic boundary conditions in the z direction by

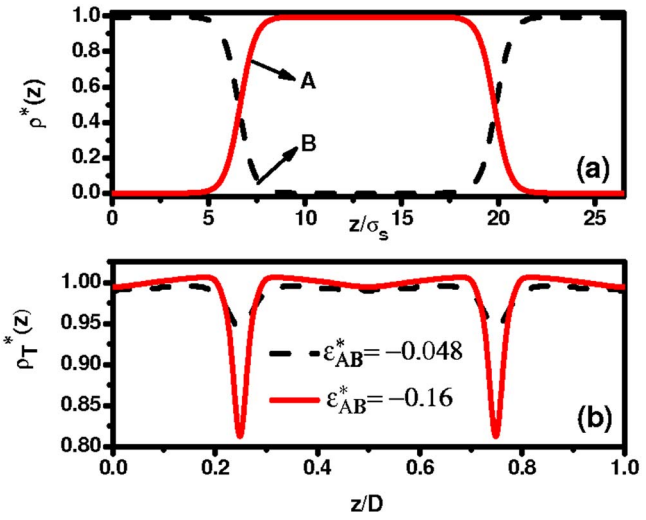

FIG. 1. (Color online) (a) The density profiles of the polymeric segments ("A" and "B") within one periodic spacing of the lamellar structure. Here $\varepsilon^*_{AA}=\varepsilon^*_{BB}=0$, $\varepsilon^*_{AB}=-0.048$, and the microdomain spacing is $D=26.5\sigma_s$. (b) Effect of the polymer incompatibility on the total local polymer density. For $\varepsilon^*_{AB}=-0.16$, the microdomain spacing is $D=36\sigma_s$. In both cases, the polymer chain length is $N=100$, and the average packing fraction is $\eta=0.35$.

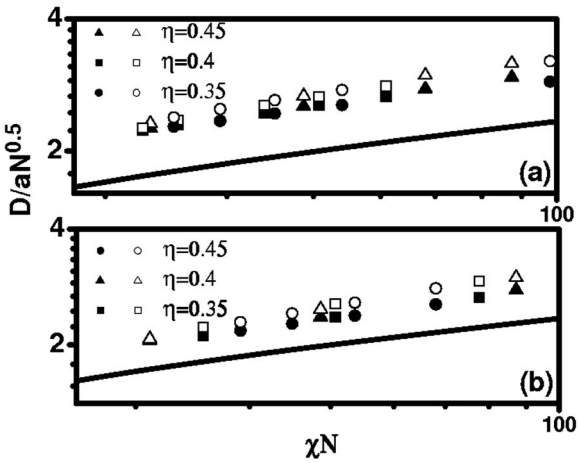

FIG. 2. The reduced periodic spacing of the lamellae ($D/aN^{0.5}$) vs χN. (a) $N=10$ and (b) $N=20$. Closed symbols are simulation results from Ref. 15, open symbols are from the DFT, and the solid lines are from the SCFT.

using the standard Picard iteration. The periodic spacing D is determined by minimization of the Helmholtz energy,[22–25] which is calculated from the polymer density profiles.

In the limit of low particle concentration, the distribution of nanoparticles within the block-copolymer network can be determined by the free energy to insert a single nanoparticle. This free energy is equivalent to the reversible work to bring the particle from an ideal-gas state to the polymer. According to the PDT,[26,27] the free energy of insertion, $W(z)$, can be calculated from the excess chemical potential of the particles, i.e.,

$$W(z) = \mu_p^{\mathrm{ex}}(z) = \frac{\delta F_{\mathrm{ex}}}{\delta \rho_p(z)}, \tag{9}$$

where the functional derivative must be evaluated from the excess Helmholtz energy for the particle-polymer mixture. Once we have the polymer density profiles calculated from the DFT for neat copolymers, Eq. (9) allows us to calculate the partitioning of particles within the polymer structure. While the density profile of the particle vanishes, it has a finite excess chemical potential in the polymer matrix.

III. RESULTS AND DISCUSSION

A. Lamellar structure

To test the numerical performance of the DFT, we first compare the lamellar morphologies of symmetric diblock copolymers with those reported by simulations.[15] In calculating the lamellar structure, we fix the average density of the diblock copolymers and apply the periodic boundary conditions to the direction perpendicular to the lamellar interface (z direction). At a given temperature and an overall polymer packing density, the lamellar thickness is identified by minimization of the Helmholtz energy.[22–25]

Figure 1 shows typical reduced density profiles of A and B segments and the total reduced density within one periodic spacing of the lamellar structure. Throughout this work, the reduced density is defined as the local density divided by the average density in the bulk. The lamellar structure is induced by the chemical incompatibilities between different blocks. Because the entropy of mixing is relatively small,[28] even a minor chemical or structural disparity between A and B blocks may result in enthalpic incompatibility sufficient for the microscopic phase separation. Figure 1 indicates that, as predicted by Monte Carlo simulations[29] and by previous DFT calculations,[22,30] the overall density is not uniform, in particular, at the microdomain interface [see Fig. 1(b)]. The slight reduction of the overall polymer density in the center of A or B microdomains can be attributed to the polymer-brush-like interactions. As discussed later, the reduction of the overall density at the interface plays a significant role in determining the nanoparticle distributions.

The microsegregation of block copolymers is often characterized by the "Flory energy parameter,"[28,15] which can be estimated from the intersegment energy parameters,

$$\chi^{\mathrm{AB}} = (n/k_BT)[\varepsilon_{\mathrm{AB}} - (\varepsilon_{\mathrm{AA}} + \varepsilon_{\mathrm{BB}})/2], \tag{10}$$

where n is the number of nonbonded neighbors within the interaction distance and ε_{ij} is the interaction energy between components i and j. For $\varepsilon_{\mathrm{AA}}=\varepsilon_{\mathrm{BB}}=0$, Eq. (10) reduces to $\chi_{\mathrm{AB}}=n\varepsilon_{\mathrm{AB}}/k_BT$. As χ_{AB} or the reduced energy $\varepsilon^*_{\mathrm{AB}}=\varepsilon_{\mathrm{AB}}/k_BT$ increases (stronger repulsion between segments of different blocks), Fig. 1(b) shows that the lamellar interface becomes more distinctive, leading to microdomains of nearly pure A or B blocks. The sharpened interface and stronger depression of polymer density suggest that nanoparticles are more likely localized in the strong segregation limit.

Figure 2 compares the theoretical predictions with the simulation results for the periodic spacing of symmetric diblock copolymers with different chain lengths and packing densities. Here $a=\sigma_s$ stands for the Kuhn length of the block copolymer and $aN^{0.5}$ represents the polymer radius of gyration estimated from the ideal-chain model ($R_g^2=\sigma_s^2N/6$). Because of the effective repulsion between AB segments, the lamellar thickness increases with the interaction energy or incompatibility. Both the DFT and simulation results suggest

that in dimensionless units, the lamellar thickness $D/(aN^{0.5})$ is mainly determined by the incompatibility parameter χN, little affected by the packing density.[15] In comparison with the simulation results, the DFT slightly overpredicts the lamellar thickness. The discrepancy may be attributed to the use of the cavity correlation function of a hard-sphere fluid to represent the correlation due to the chain connectivity or to the mean-field approximation for the van der Waals attractions. The theoretical performance can be improved by using the correlation functions for the square-well fluids.[31]

The SCFT predicts that the lamellar thickness is a universal function of the incompatibility parameter χN, independent of either the polymer packing density or the polymer chains. The difference between SCFT and DFT/simulation results is probably due to the use of the incompressible model in this work. Distinct from the SCFT, both the DFT and simulation indicate that the reduced lamellar thickness $[D/(aN^{0.5})]$ depends not only on the incompatibility parameter χN but also on the polymer chain length.

B. Particle distributions

In the limit of low particle density, the probability of particle distribution follows the Boltzmann law[13]

$$p(z) \propto \exp[-\beta W(z)], \tag{11}$$

where $W(z)$ is the reversible work to insert a particle in a lamellar structure of block copolymers. The proportionality coefficient can be determined from the condition of normalization,

$$\int_0^D p(z)dz = 1. \tag{12}$$

Because $W(z)$ is related to the excess chemical potential of the particle in the mixture, Eq. (11) suggests that the distribution of nanoparticles depends not only on the particle size and surface energy but also on the local structure of the block copolymer.

To distinguish the different effects of particle size and interaction energy on the partitioning function, we first consider the distribution of neutral particles, i.e., $\varepsilon^*_{AP}=\varepsilon^*_{BP}=0$, in the lamellae of block copolymers. In the absence of energetic preference, previous theoretical investigations suggest that the composite structure is dominated by the entropy effect, i.e., by the effect of particle on the local polymer conformation.

1. Distribution of neutral particles

Effect of particle size. Figure 3 shows the density distributions of polymer segments and of neutral particles of different sizes within one periodic length of the lamellar structure. Here the polymer chain length is $N=100$, the radius of gyration is $4\sigma_s$, the microdomain thickness is $L=10\sigma_s$, and the interfacial width is about $\delta=1.3\sigma_s$ (defined as the half peak width of the overall density). Figure 3(b) shows that, as observed in experiments,[11,12] small particles (ratio of the particle radius to the segment length $R/\sigma_s=2$) favor the microdomain interface while large particles prefers the interior regions ($R/\sigma_s=14$). The distribution is nearly uniform for very small particles ($R/\sigma_s=0.4$). Qualitatively, these results are in good agreement with the previous SCFT/DFT predictions.[32]

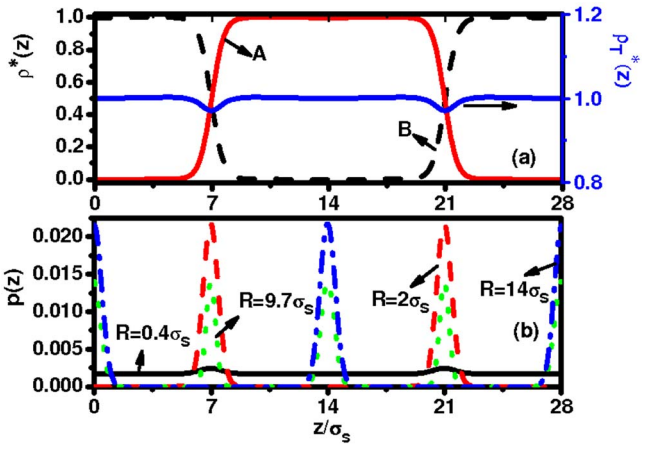

FIG. 3. (Color online) (a) The density profiles of the polymeric segments (A and B) and the total polymer density within one period of the lamellae. Here the average packing fraction of the polymer is $\eta=0.42$, the energy parameters are $\varepsilon^*_{AA}=\varepsilon^*_{BB}=0$, $\varepsilon^*_{AB}=-0.048$, and the periodic spacing is $D=28\sigma_s$. (b) The distribution probability of neutral particles with different radii (R) in the block-copolymer lamellae.

We find that a neutral particle is almost exclusively located at the lamellar interface if its size is comparable to the thickness of the density depression well (δ). Intuitively, the reduced density at the interface helps accommodation of the particle. The particle accumulation at the lamellar interface can also be explained by the reduction of the number of AB contacts or the interfacial tension.[13]

Figure 3(b) suggests that the preference of the particles at the microdomain interface is not linearly dependent on the size. Interestingly, a neutral particle may have equal probability to locate at the interface or at the domain center (e.g., $R=9.7\sigma_s$). It favors the microdomain interface if the particle radius $R<9.7\sigma_s$ ($9.7\sigma_s$ is approximately the same as the domain size L), but the particle is preferentially located at the center of a microdomain if its size $R>9.7\sigma_s$ [such as $R=14\sigma_s$ in Fig. 3(b)]. As indicated by Balazs and co-workers,[5,33] the particle distribution is determined by a competition of the translational entropy with the chain configurational entropy. Introduction of small particles (with radii $R \ll L$) into the lamellar structure leads to the interfacial segregation, while large particles, i.e., when the radii are close to the thickness of the host domain, accumulate in the domain center. These predictions have also been confirmed by experiments.[1,12,32,34]

Center-interface preference. The difference in the insertion free energies at the lamellar interface and at the microdomain center provides an effective measure of the particle preference,

$$\delta\beta W = \beta(W_{\text{interface}} - W_{\text{domain}}). \tag{13}$$

If $\delta\beta W<0$, the particle prefers the interface; while for $\delta\beta W>0$, the particle prefers the microdomain center. Figure 4(a) shows that the relative insertion energy oscillates with the variation of the particle diameter, with a periodicity comparable to the domain size. The maximum/minimum values of $\delta\beta W$ correspond to the conditions of strong localization,

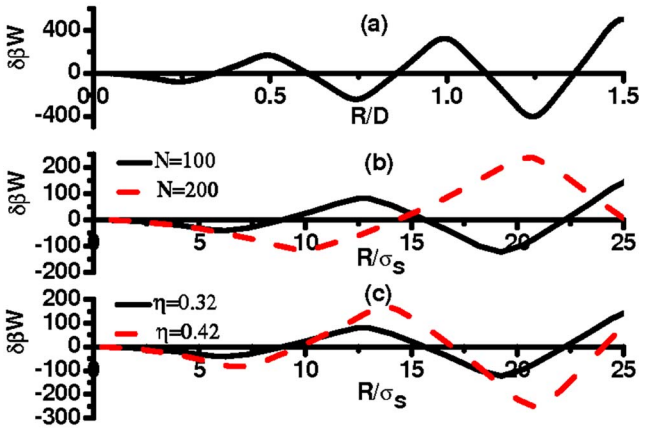

FIG. 4. (Color online) (a) Dependence of the biased one-particle potential $\delta\beta W$ on the ratio of the particle radius to the lamellar periodic spacing (R/D). All parameters for the copolymers are identical to those shown in Fig. 3(a). (b) Effect of the chain length on the biased one-particle potential $\delta\beta W$. (c) Effect of the polymer density on $\delta\beta W$.

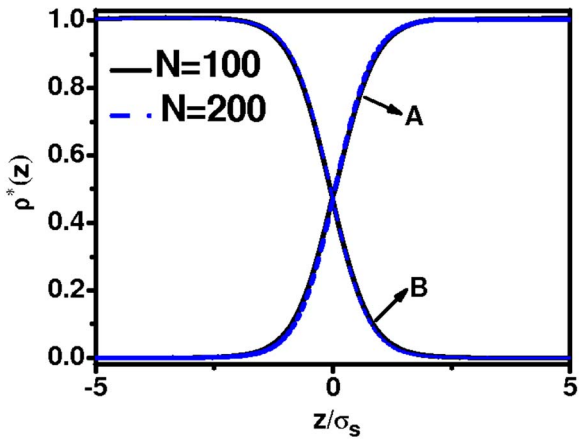

FIG. 5. (Color online) Effect of the chain length on the local structure of lamellar interface (the interface is $z=0$).

i.e., accumulation of the particles at the microdomain center or interface. Because the magnitude of the insertion energy increases with the particle size, Fig. 4(a) predicts that large particles are more easily localized in different positions of the lamellar structure.

Figure 4(b) compares the relative preference of a neutral particle at the interface or at microdomain center for the two lamellae with different block copolymer chain lengths ($N=100$ and $N=200$). Both profiles exhibit a periodic oscillation of the particle distribution with respect to the particle size with the periodicity comparable to the domain size. For a small neutral particle ($R<5\sigma_s$), the relative insertion energy $\delta\beta W$ is independent of the chain length. This verifies an earlier conclusion from Figs. 3 and 4(a) that the density depression at the interface plays a prominent role for the distribution of small particles, independent of the lamellae thickness. As the particle size increases, however, the relative insertion potential is strongly affected by the lamellar thickness, leading to the oscillatory structure.

Figure 4(c) compares the relative preference of neutral particles at the interface or at microdomain center for two lamellae with different packing fractions ($\eta=0.32$ and $\eta=0.42$). As discussed earlier, the particle distribution function exhibits oscillatory preference of microdomain center or interface, depending on its size. At different packing densities, the periodicities of the oscillation ($\delta\beta W$ versus R/σ_s) are different; each is dictated by its own lamellar periodic spacing.

Effect of polymer chain length. We now consider the effect of the polymer chain length on the particle distribution by increasing the chain length from $N=100$ to 200. According to Eq. (10), the segregation parameter corresponds to $\chi_{AB}N\approx 30$ for $N=100$ and 60 for $N=200$ (assuming the number of nearest neighbors $n=6$). At the same polymer packing density, the periodic spacing of the lamellae expands from $D=26\sigma_s$ to $41.5\sigma_s$. Figure 5 indicates that the chain length has only negligible effects on the lamellar interfacial structure. The sharp interface can be explained by the strong segregation conditions considered in this work. The effect of chain length on the interfacial profile would be more prominent at the weak polymer segregation limit ($\chi_{AB}N\sim 10$), e.g., for lamellae composed of short-chain copolymers, which has been verified by recent simulation results.[35]

Figure 6(a) shows the distribution function of a small particle (e.g., $R=5\sigma_s$) near the microdomain interface. The embedded figure shows the overall density profile within the same lamellae. As the chain length increases, the overall density exhibits a more pronounced depression at the interface, leading to a stronger localization of small particles. For $N=200$, Fig. 6(b) shows localization of large particles ($R=15\sigma_s$) at the center of A microdomain, which can be explained by the fact that the ratio of the domain width to the lamellar periodic spacing decreases as the polymer chains become longer. As indicated earlier, the degree of the particle localization is sensitive to the relative size (R/σ_s) of the particle and the periodic spacing of the lamellae.

Effect of polymer compressibility. In comparison with the SCFT, one advantage of the DFT is that it is able to explicitly account for polymer compressibility. To explore the effect of polymer density on the particle distribution, we increase the packing fraction of the block polymer from 0.32

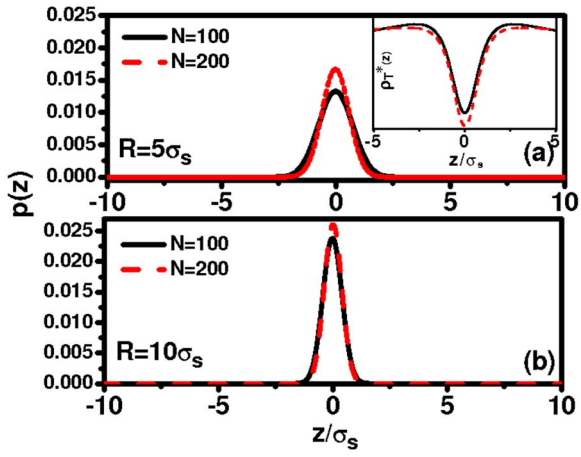

FIG. 6. (Color online) Effect of the chain length on the distribution of small $(a, R=5\sigma_s)$ and large $(b, R=15\sigma_s)$ neutral particles. The peaks in the particle distribution functions are aligned at $z=0$. The embedded figure represents the reduced total density profile at the interface.

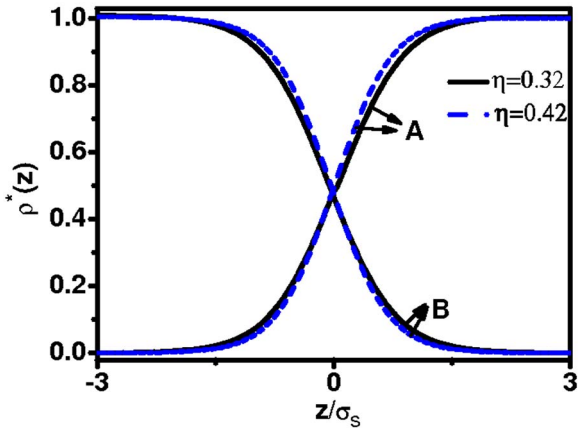

FIG. 7. (Color online) Effect of the overall packing density on the local structure of lamellar interface.

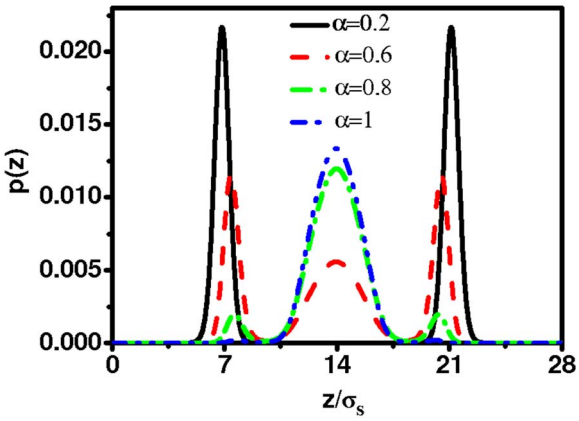

FIG. 9. (Color online) Effect of the energetic selectivity on the particle-distribution probability. Here the particle radius is $R=2\sigma_s$; all parameters for the polymers are identical to those shown in Fig. 3(a).

to 0.42. The increase in density results in a slight increase of the lamellar spacing from $D=26\sigma_s$ to $28\sigma_s$. However, as shown in Fig. 7, the change in packing density has only negligible effect on the lamellar interfacial density profile, except that the boundary at the interface becomes more distinctive at the higher packing density.

Figure 8(a) shows the distribution function of a small particle (e.g., $R=7\sigma_s$) around the lamellar interface. We find that the particle is more localized as the packing density increases. At a fixed chain length, the lamellar interfacial tension is directly proportional to the packing density.[13] The increase in the packing density leads to a higher interfacial tension, which drives the enhanced localization of small particles at the interface. Figure 8(b) shows that a larger particle (e.g., $R=14\sigma_s$) magnifies localization at the domain center, which is probably due to the reduced domain center width/lamellar periodic spacing as the packing density increases.

2. Distribution of energetically selective particles

Effect of surface energy. We now consider the effect of particle surface energy on the distribution probability in the lamellar structure. Recent experiments demonstrated that the particle location can be effectively controlled by tailoring its chemical affinity to a specific domain of the copolymer.[9,10] For example, it has been shown that particles are localized in one particular microdomain if they are coated with short homochains with the repeating units identical to those of polymer block. To investigate the effect of surface energy, we calculate the particle distribution probability at different values of the energy selectivity parameter, $\alpha=-(\varepsilon^*_{AP}-\varepsilon^*_{BP})/\varepsilon^*_{AB}$. Figure 9 shows that as the particle becomes energetically more selective, its central position shifts from the interface to the center, in good agreement with recent experiments (e.g., Fig. 4 of Ref. 36) and theoretical calculations [e.g., Fig. 1(a) of Ref. 13]. Depending on the surface energy, the particle distribution function varies from one peak at A domain ($\alpha=1$) to three peaks ($\alpha=0.6$) at both domain center and interfaces, and finally to two peaks at the interfaces ($\alpha=0.2$). The variation of peak position shows a strong interplay of the particle size and surface energy. Figure 9 suggests that by an effective control of the surface energy and particle size, one may manipulate the particle distribution and thereby the morphology of the nanocomposite.

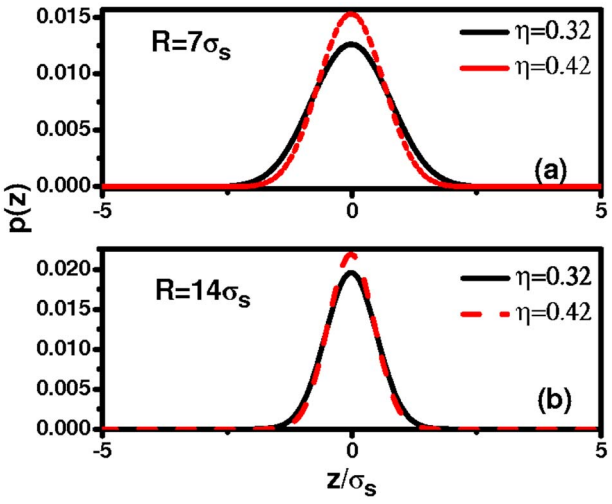

FIG. 8. (Color online) (a) The probability distribution function for a small neutral particle ($R=7\sigma_s$) at the lamellar interface ($z=0$). (b) The probability distribution function for a large neutral particle ($R=14\sigma_s$) at the center of the A domain ($z=0$).

Effect of particle size. To further examine the interplay of particle size and energy effects, we calculate the density distributions of particles with different sizes but the same selectivity parameter α. For energetically selective particles, the particle position is determined by a competition in decreasing the AB interfacial tension due to localization of the particles and in decreasing the energy by localizing the particle at the center of A microdomain. Figure 10(a) shows that, for particles with relatively low biased energy ($\alpha=1$), small particles ($R=0.8\sigma_s$) distribute nearly uniformly within the A microdomain, with a slightly higher probability at the interface. The distribution becomes more inhomogeneous as the particle size increases. When the particle size is beyond $R=2.4\sigma_s$, a counterbalance of the enthalpic and entropic effects makes the particle preferentially reside at the domain center (e.g., $R=4\sigma_s$). At $R=6\sigma_s$, the particle distribution function exhibits two strong peaks near the lamellar interface. Because of the combined effects of interfacial energy and microdomain affinity, we expect that beyond certain size,

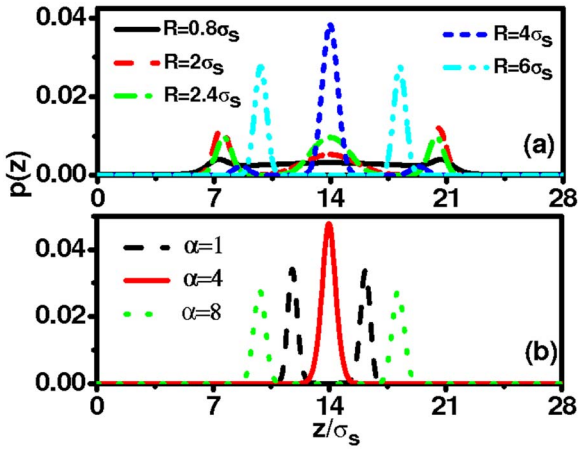

FIG. 10. (Color online) (a) The probability distribution functions for particles of different sizes at $\alpha=1$. (b) Effect of the selectivity parameter on the particle distribution at $R=6\sigma_s$. All parameters for the polymers are the same as those shown in Fig. 3(a).

the particle position can be effectively controlled by the particle-polymer interactions.

Figure 10(b) shows the distribution function of a particle with radius $R=6\sigma_s$ at different degrees of affinity to the A domain. As the degree of selectivity increases, the particle moves from the region near the lamellar interfaces to the center of the A domain. Different from simulation results, nanoparticles of different energy affinities may form monolayer sheets in the center of the preferred microdomain or bilayer sheets with one sheet next to each lamellar interface.[37]

Effect of polymer chain length. Figure 11 shows the effect of the polymer chain length on the particle distribution function at two different surface energies. When $\alpha=1$, the particle shows equal preference at the microdomain interface and at the domain center but when $\alpha=4$, it favors the center due to the dominant energy effect. At the same ratio of the particle radius to the lamellar thickness (R/D), the particle distribution functions are similar over the entire range of z/D. The difference in the magnitude is due to the effect of the particle size. Figure 9 affirms that the distribution of the particle in the block copolymer depends on the particle-polymer relative size and the particle surface energy.

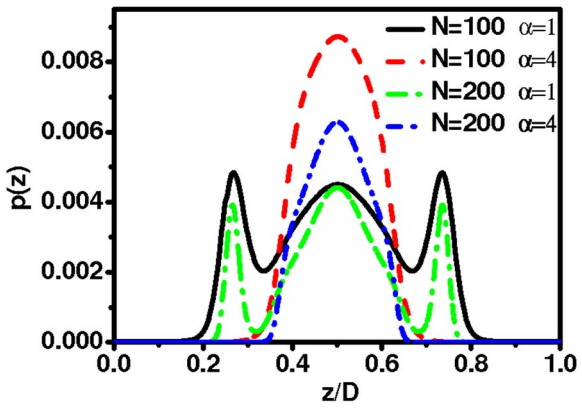

FIG. 11. (Color online) Effect of the chain length on the distributions of energetically selective nanoparticles $(R/D=0.05)$.

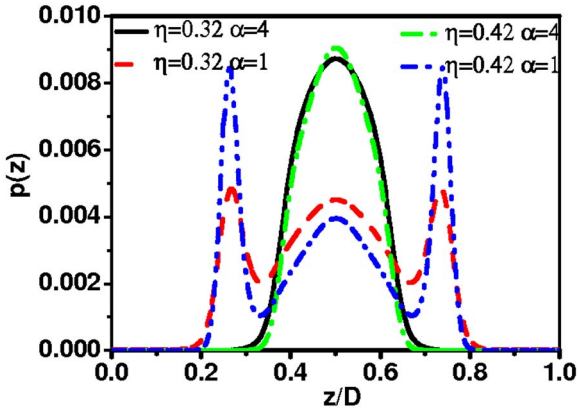

FIG. 12. (Color online) Effect of the chain length on the probability distribution functions for nanoparticles with different selectivity parameters. Here the particle size is fixed relative to the periodic spacing $(R/D=0.05)$.

Effect of polymer compressibility. Figure 12 shows the effect of the polymer packing density on the particle distribution probability at two different surface energies. When $\alpha=1$, the particle shows nearly equal preference to the interface and to the center of A microdomain at the lower packing density $(\eta=0.32)$, but favors the interface at the higher packing density $(\eta=0.42)$. For particles with strong energetic preference $(\alpha=4)$, however, the A microdomain is favored for both cases, suggesting that the particle location is sensitive to both the energy and packing effects. According to Fig. 12, one may effectively control the particle location by varying the surface energy or packing density or both without changing the particle size.

IV. CONCLUSIONS

The distribution of nanoparticles in the lamellae of symmetric block copolymers depends on a number of parameters including the lamellar thickness and interfacial structure, the particle/polymer size ratio, and the interactions between copolymer and nanoparticles. It is a combination of all these factors that determine the morphology of block copolymer-particle composites.

In this work, we provide theoretical predictions about the nanoparticle distribution in the lamellar structure of symmetric diblock copolymer by combining a nonlocal density functional theory for the polymer structure with the potential distribution theory for the particle distributions. It appears that the theory is able to capture all important parameters affecting the microscopic structure. Although the calculations are focused on the dilute limit, we expect that the same theoretical framework is applicable to composites of finite particle concentration.

Approximately, there are three scenarios for the distribution of neutral particles in the lamellae of symmetric block copolymers. Without the energetic preference, small particles distribute nearly uniformly throughout the lamellar structure, exhibiting only a slightly enhanced probability at the interface. Particles with the diameter comparable to the interfacial thickness are located primarily within the depression well of the overall density. Larger particles may strongly accumulate at the interface or at the microdomain centers, depending on

the periodicity of the lamellae. Different from previous investigations, we find that the reduction of the overall density at the lamellar interface plays a central role in determining the distribution of neutral particles.

Introduction of energy preference leads to accumulation of particles into a particular microdomain. The distribution is nearly uniform for small particles but centralized for large particles. Particles with intermediate size may form layered structure within the energetically biased microdomain. At the same packing density, the polymer chain length has little effect on the particle distribution if its size is expressed relative to the periodic spacing of the lamellae. A variation of the polymer density, however, may result in significant changes in the particle distributions.

ACKNOWLEDGMENTS

The authors are thankful to Zhidong Li for insightful discussions, to Carol K. Hall and Andrew J. Schultz for providing the simulation results, and to Mark Matsen for providing results from the self-consistent theory. This research is sponsored by the U.S. Department of Energy (DE-FG02-06ER46296) and uses the computational resources from the National Energy Research Scientific Computing Center (NERSC), which is supported by the Office of Science of the U.S. Department of Energy under Contract No. DE-AC03-76SF0009.

APPENDIX: EXCESS HELMHOLTZ ENERGY FUNCTIONAL

The excluded-volume Helmholtz energy takes into account contributions from both the nanoparticles and the polymer segments. According to a modified fundamental measure theory,[18,19] $\phi^{\mathrm{hs}}[n_\alpha(\mathbf{r})]$ is given by

$$\beta\phi^{\mathrm{hs}} = -n_0\ln(1-n_2) + \frac{n_1 n_2 - \mathbf{n}_{V1}\mathbf{n}_{V2}}{1-n_3} + \frac{1}{36\pi}\left[n_3\ln(1-n_3) + \frac{n_3^2}{(1-n_3)^2}\right] \times \frac{(n_2^3 - 3n_2\mathbf{n}_{V2}\mathbf{n}_{V2})}{n_3^3}, \quad \text{(A1)}$$

where $n_\alpha(r)$, $\alpha=0,1,2,3,V_1,V_2$, are weighted densities that are defined by the densities of the particles and block copolymers

$$n_\alpha(\mathbf{r}) = \sum_j n_{\alpha j}(\mathbf{r}) = \sum_j \int \rho_j(\mathbf{r}')\omega_j^\alpha(\mathbf{r}-\mathbf{r})d\mathbf{r}' \quad \text{(A2)}$$

where ω_j^α ($\alpha=0,1,2,3,V1,V2$) are weight functions.[20]

The effect of chain connectivity on the intersegmental correlations is represented by an extended thermodynamic perturbation theory,[18]

$$\beta\phi^{\mathrm{chain}}(n_\alpha) = \frac{1-M}{M} n_{0,S}\xi_S \ln y^{\mathrm{hs}}(\sigma, n_\alpha), \quad \text{(A3)}$$

where M represents the number of segments per polymer chain, subscript S designates polymer segments, $\xi_S = 1 - \mathbf{n}_{V_{2,S}}\cdot\mathbf{n}_{V_{2,S}}/n_{2,S}^2$, and $y^{\mathrm{hs}}(\sigma,n_\alpha)$ is the contact value of the cavity correlation function of a hard-sphere reference,

$$y^{\mathrm{hs}}(\sigma,n_\alpha) = \frac{1}{1-n_3} + \frac{n_2\xi\sigma}{4(1-n_3)^2} + \frac{n_2^2\xi_S\sigma}{72(1-n_3)^3}. \quad \text{(A4)}$$

Finally, the van der Waals attraction is represented by the mean-field approximation

$$\beta F_{\mathrm{ex}}^{\mathrm{sw}}[\{\rho_j(\mathbf{r})\}] = \frac{1}{2}\int\int d\mathbf{r}d\mathbf{r}' \times \sum_{i,j\in P,A,B} \rho_i(\mathbf{r})\rho_j(\mathbf{r})\beta\varphi_{ij}^{\mathrm{att}}(|\mathbf{r}-\mathbf{r}'|), \quad \text{(A5)}$$

where $\varphi_{ij}^{\mathrm{att}}(r)$ is given by Eq. (1) in the text.[16]

[1] M. R. Bockstaller, R. A. Mickiewicz, and E. L. Thomas, Adv. Mater. (Weinheim, Ger.) **17**, 1331 (2005).
[2] Y. Lin, A. Boker, J. B. He, K. Sill, H. Q. Xiang, C. Abetz, X. F. Li, J. Wang, T. Emrick, S. Long, Q. Wang, A. Balazs, and T. P. Russell, Nature (London) **434**, 55 (2005).
[3] Q. Wang, P. F. Nealey, and J. J. de Pablo, J. Chem. Phys. **118**, 11278 (2003).
[4] A. C. Balazs, T. Emrick, and T. P. Russell, Science **314**, 1107 (2006).
[5] R. B. Thompson, V. V. Ginzburg, M. W. Matsen, and A. C. Balazs, Science **292**, 2469 (2001).
[6] R. B. Thompson, V. V. Ginzburg, M. W. Matsen, and A. C. Balazs, Macromolecules **35**, 1060 (2002).
[7] J. Y. Lee, Z. Shou, and A. C. Balazs, Phys. Rev. Lett. **91**, 136103 (2003).
[8] R. B. Thompson, J. Y. Lee, D. Jasnow, and A. C. Balazs, Phys. Rev. E **66**, 031801 (2002).
[9] J. J. Chiu, B. J. Kim, E. J. Kramer, and D. J. Pine, J. Am. Chem. Soc. **127**, 5036 (2005).
[10] B. J. Kim, S. Given-Beck, J. Bang, C. J. Kawker, and E. L. Thomas, Macromolecules **40**, 1796 (2007).
[11] M. R. Bockstaller and E. L. Thomas, Phys. Rev. Lett. **93**, 166106 (2004).
[12] M. R. Bockstaller, Y. Lapetnikov, S. Margel, and E. L. Thomas, J. Am. Chem. Soc. **125**, 5276 (2003).
[13] V. Pryamitsyn and V. Ganesan, Macromolecules **39**, 8499 (2006).
[14] S. W. Sides, B. J. Kim, E. J. Kramer, and G. H. Fredrickson, Phys. Rev. Lett. **96**, 250601 (2006).
[15] A. J. Schultz, C. K. Hall, and J. Genzer, J. Chem. Phys. **117**, 10329 (2002).
[16] D. P. Cao and J. Z. Wu, J. Chem. Phys. **126**, 144912 (2007).
[17] D. P. Cao and J. Z. Wu, Macromolecules **38**, 971 (2005).
[18] Y. X. Yu and J. Z. Wu, J. Chem. Phys. **117**, 10156 (2002).
[19] R. Roth, R. Evans, A. Lang, and G. Kahl, J. Phys.: Condens. Matter **14**, 12063 (2002).
[20] Y. Rosenfeld, J. Phys.: Condens. Matter **14**, 9141 (2002).
[21] Z. D. Li, D. P. Cao, and J. Z. Wu, J. Chem. Phys. **122**, 174708 (2005).
[22] A. L. Frischknecht, J. G. Curro, and L. J. D. Frink, J. Chem. Phys. **117**, 10398 (2002).
[23] K. R. Shull, Macromolecules **25**, 2122 (1992).
[24] A. L. Frischknecht and J. D. Weinhold, A. G. Salinger, J. G. Curro, L. J. D. Frink, and J. D. McCoy, J. Chem. Phys. **117**, 10385 (2002).
[25] A. L. Frischknecht, J. G. Curro, and L. J. D. Frink, J. Chem. Phys. **117**, 10398 (2002).
[26] J. R. Henderson, Mol. Phys. **50**, 741 (1983).
[27] R. Roth, R. Evans, and S. Dietrich, Phys. Rev. E **62**, 5360 (2000).
[28] F. S. Bates and G. H. Fredrickson, Phys. Today **52**(2), 32 (1999).
[29] Q. A. Wang, Q. L. Yan, P. F. Nealey, and J. J. de Pablo, J. Chem. Phys. **112**, 450 (2000).
[30] S. K. Nath, J. D. McCoy, J. G. Curro, and R. S. Saunders, J. Chem. Phys. **106**, 1950 (1997).

[31] Y. P. Tang and B. C. Y. Lu, J. Chem. Phys. **100**, 6665 (1994).
[32] J. Y. Lee, R. B. Thompson, D. Jasnow, and A. Balazs, Macromolecules **35**, 4855 (2002).
[33] J. Huh, V. V. Ginzburg, and A. C. Balazs, Macromolecules **33**, 8085 (2000).
[34] J. U. Kim and B. O'Shaughnessy, Phys. Rev. Lett. **89**, 238301 (2002).
[35] Q. Sun and R. Faller, J. Chem. Phys. **126**, 144908 (2007).
[36] B. Kim, J. Bang, C. Hawker, and E. Kramer, Macromolecules **39**, 4108 (2006).
[37] A. J. Schultz and C. K. Hall, Macromolecules **38**, 3007 (2005).